Precision x-ray crystal spectroscopy of neonlike gold

G. A. Chandler, M. H. Chen, D. D. Dietrich, P. O. Egan, and K. P. Ziock
University of California, Lawrence Livermore National Laboratory, Livermore, California 94550

P. H. Mokler and S. Reusch
Gesellschaft für Schwerionenforschung (GSI), D-6100 Darmstadt, Federal Republic of Germany

D. H. H. Hoffmann
Max-Planck-Institute for Quantum Optics (MPQ), D-8046 Garching, Federal Republic of Germany
(Received 21 July 1988)

The spectrum of neonlike gold (+69) is observed in a beam-foil light source utilizing an x-ray crystal spectrograph. Precision wavelength determinations indicate variations from multiconfigurational Dirac-Fock calculations for states sampling the 2*s* hole states consistent with previous observations in bismuth (+73).

The spectra of highly ionized Ne-like atomic systems are of interest for many reasons, including plasma diagnostics[1] and as tests of theoretical multielectron atomic physics models. We have previously observed the x-ray spectra of Ne-like bismuth (net charge = +73),[2] lanthanum (+47) and rhodium (+35),[3] and xenon (+44),[4] using beam-foil spectroscopy. Here we present the beam-foil x-ray spectrum of Ne-like gold (+69). The data show variations from theoretical multiconfiguration Dirac-Fock (MCDF) $n=3$-2 transition energy calculations consistent with those previously observed in our bismuth spectrum for the states which have the largest quantum electrodynamic (QED) contributions.

The experimental technique used has been previously reported[2] and will only be briefly discussed here. Gold ions with a charge of +36 and a nominal beam energy of 15 MeV/amu are produced at the UNILAC heavy-ion accelerator at the Gesellschaft für Schwerionenforschung (GSI) in Darmstadt, West Germany. In our experimental area the ions impinge on a thick stripper foil of 2.8 mg/cm^2 of beryllium to achieve charge-state equilibrium. The equilibrium charge-state distribution is not measured in this experiment; however, the semiempirical fits of Nikolaev and Dmitriev[5] yield a charge-state distribution peaked between the Na-like and Mg-like charge states. This is shown in Fig. 1, and is consistent with the spectral line intensities observed.

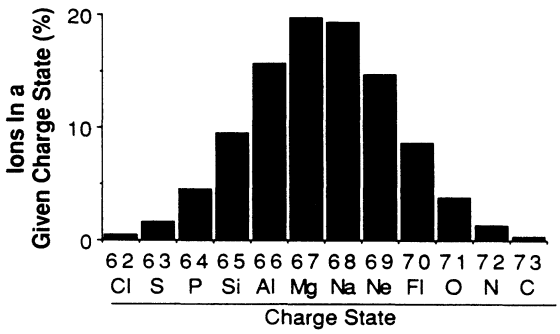

FIG. 1. This figure shows the calculated charge-state equilibrium for gold ions at 15 MeV/amu.

This charge-state distribution then passes through a carbon exciter foil (570 mg/cm^2) located in our instrument where the subsequent x-ray emission from the ions is viewed by two Johann curved-crystal spectrographs and a lithium-drifted silicon [Si(Li)] detector. The two crystal spectrographs view the x-ray emission nominally perpendicular to the relativistic ion beam, and in such a way as to compensate for a linear Doppler shift of the x rays, as observed by each spectrograph, by simply averaging the spectra recorded by both instruments. The spectra were normalized to the total measured charge as collected in an unbiased Faraday cup. Total exposures of 10 mC were used to obtain the spectra with average beam currents of ~500 nA (8 particle nA).

In Fig. 2 the Si(Li) spectrum observed is shown with

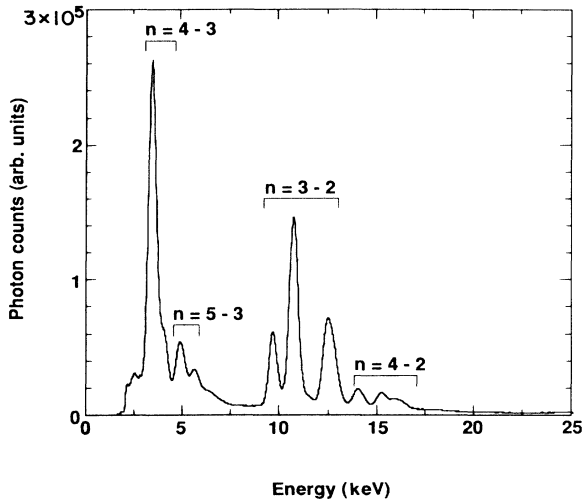

FIG. 2. Si(Li) spectrum of 15-MeV/amu gold ions passing through a 570-μg/cm^2 carbon foil taken after they passed through a 2.8-mg/cm^2 beryllium stripper foil. Transitions are predominantly from $n=4$-3 and $n=5$-3 transitions in Na-like and Mg-like ions and $n=3$-2 and $n=4$-2 transitions in Ne-like, Na-like, and Mg-like ions.

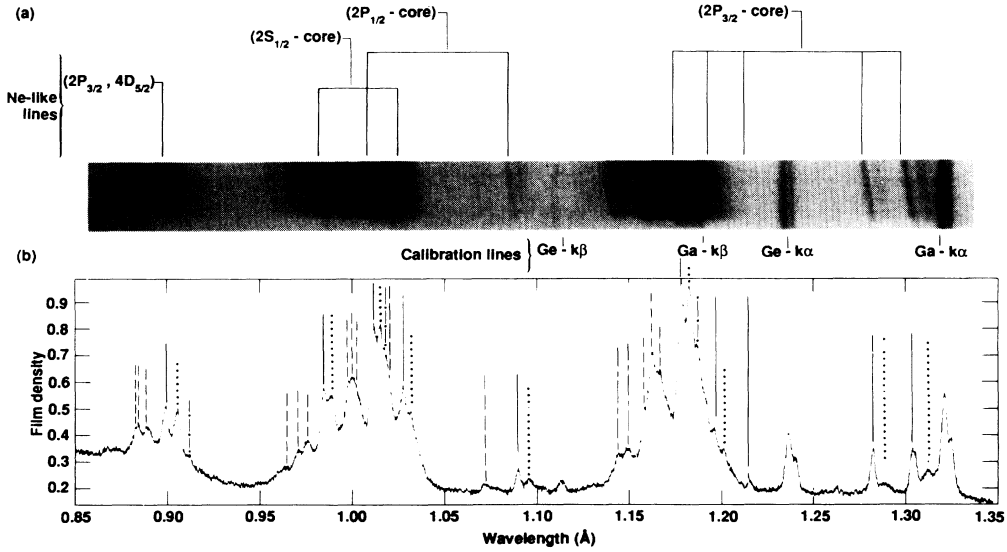

FIG. 3. (a) Raw film data of a gold x-ray spectrum taken with an indium antimony 220 crystal. (b) A densitometer trace of the spectrum formed by averaging densitometer scans along the gold x-ray lines. The lines are identified from a given charge state in the spectra as follows: ——, Ne-like; · · · ·, Na-like, —·—·—·, Mg-like; — — —, F-like; ------ and O-like.

the energy scale corrected for the Doppler shift of the lines. The low-energy peaks are predominantly from $n=4$-3 and $n=5$-3 transitions in Na-like and Mg-like gold. The higher-energy peaks are due to Ne-like $n=3$-2 and $n=4$-2 transitions and their satellite lines which are well resolved in the x-ray crystal spectrum, as shown in Fig. 3(a). The spectrum was recorded using Kodak direct exposure film (DEF). Two different crystals were used in the experiment—indium antimony (InSb) 220 and germanium (Ge) 220. The spectrographs used have a 1-m Rowland circle radius and a Bragg angle coverage between 10° and 18°. The resolution observed using the Ge crystals was approximately a factor of 2 better than that observed with the InSb crystals, $I/\Delta I \sim 800$ vs 400, but the two longest-wavelength Ne-like lines were out of the dispersion range when using the Ge crystals.

The calibration for each spectrum is found by fitting the dispersion relation to gallium, germanium, bromine, and yttrium x-ray lines produced by electron-beam bombardment of a mixture of Ga_2O_3, Ge, $SrBr_2$, and Y powders in a specially designed x-ray tube. From the instrument geometry and the projection of wire shadows onto the film planes, the dispersion relation can be uniquely defined for the Doppler shifted x-ray lines from the gold ions. These lines are observed to be tilted along the dispersion axis, as shown in Fig. 3(a). This effect is due to the linear Doppler shift of the x rays from the relativistic gold ions ($v/c \sim 0.175$) as a function of the crystal height.

The crystal spectrum consists of features predominantly from the $n=3$ and 4-2 transitions in the Ne-like, Na-like, and Mg-like charge states. Features in the F-like and O-like charge states are also identified. Eleven neonlike lines are listed in Table I. Ten transitions are $n=3$-2

TABLE I. Neonlike gold transition energies to the ground state (in eV).

Upper level	Measured[a]	Calculated	Difference	Rel. int.	$(2J+1)R_b$ [b]	gf
$(2p_{3/2},3s_{1/2})_1$	9506.5(4.5)	9 505.3	1.2	0.41	3.0	$1.50E-1$
$(2p_{3/2},3p_{1/2})_2$	9666.7(4.5)	9 663.6	3.1	0.34	4.9	$1.70E-3$
$(2p_{3/2},3p_{3/2})_2$	10 190.0(4.9)	10 193.6	−3.6	0.02	1.5	$1.50E-3$
$(2p_{3/2},3d_{3/2})_1$	10 357.9(5.2)	10 363.7	−5.8	0.09	3.0	$8.90E-3$
$(2p_{3/2},3d_{5/2})_1$	10 519.7(5.4)	10 527.7	−8.0	1.00	3.0	$2.26E+0$
$(2p_{1/2},3s_{1/2})_1$	11 374.8(6.2)	11 377.5	−2.7	0.04	3.0	$2.70E-2$
$(2p_{1/2},3d_{3/2})_1$	12 260.8(7.1)	12 268.5	−7.7	0.26	3.0	$9.53E-1$
$(2s_{1/2},3p_{1/2})_1$	12 071.6(6.9)	12 081.4	−9.8	0.15	2.8	$3.43E-1$
$(2s_{1/2},3p_{3/2})_1$	12 600.2(7.5)	12 608.6	−8.4	0.06	2.8	$2.42E-1$
$(2s_{1/2},3d_{5/2})_2$	12 909.6(7.8)	12 915.8	−6.1	0.04	1.6	$1.25E-2$
$(2p_{3/2},4d_{5/2})_1$	13 802.8(8.9)	13 809.7	−6.9	0.14	1.3	$4.84E-1$

[a]Numbers in parentheses are the experimental errors.
[b]$(2J+1)R_b$ represents the level multiplicity times the branching ratio for decay.

TABLE II. Sources of measured energy errors for neonlike gold transitions (in eV).

Upper level	Statistical	Foil location (∓0.5 mm)	Crystal alignment (∓1 mrad)	Beam energy (∓1.4%)
$(2p_{3/2},3s_{1/2})_1$	1.46	2.35	0.24	1.87
$(2p_{3/2},3p_{1/2})_2$	1.51	2.43	0.24	1.72
$(2p_{3/2},3p_{3/2})_2$	1.67	2.71	0.24	1.81
$(2p_{3/2},3d_{3/2})_1$	1.73	2.81	0.24	2.04
$(2p_{3/2},3d_{5/2})_1$	1.79	2.90	0.24	2.07
$(2p_{1/2},3s_{1/2})_1$	2.09	3.40	0.24	2.24
$(2p_{1/2},3d_{3/2})_1$	2.42	3.97	0.24	2.42
$(2s_{1/2},3p_{1/2})_1$	2.35	3.85	0.24	2.38
$(2s_{1/2},3p_{3/2})_1$	2.56	4.20	0.24	2.48
$(2s_{1/2},3d_{5/2})_2$	2.69	4.51	0.25	2.29
$(2p_{3/2},4d_{5/2})_1$	3.07	5.18	0.29	2.72

transitions, including three electric quadrupole transitions, and one transition is a $n=4$-2 transition. Ne-like features corresponding to the transitions from the upper levels $(2p_{1/2},4s_{1/2})_1$, $(2p_{1/2},4d_{3/2})_1$, $(2s_{1/2},4p_{1/2})_1$, and $(2s_{1/2},4p_{3/2})_1$ to the ground state were noted but are not listed due to the poor calibration in this region of the spectrum. The notation indicates a hole state in the $n=2$ shell and an electron state in the $n=4$ shell which are coupled to give a total angular momentum, $J=1$, state. The second Ne-like electric quadrupole line, which is observed with some uncertainty due to its weakness and proximity to a Ge crystal absorption edge in the bismuth spectra, is readily apparent, although still relatively weak, in this gold spectrum. Given the weakness of this line compared with the lowest-energy $E2$ transition to the ground state, from the $(2p_{3/2},3p_{1/2})_2$ upper level, and that the gf values (statistically weighted oscillator strength) and branching ratios of the two transitions are very similar, it seems apparent that the population mechanisms for the two lines are quite different and that neither simple direct excitation nor a simple statistical population of the levels is indicated.

In Table I it is seen that the overall agreement between the measured transition energies and the present MCDF calculations, from Grant's code,[6] is quite good. These calculations have been performed using an extended average level (EAL) scheme, where the frequency-dependent Breit interaction has been included as well as QED, finite nuclear size, and relaxation corrections. In the basis-state expansion we included all the configuration-state functions from the same complex. For the $(2s,3p)_1$ state the energy shift due to Coster-Kronig fluctuation[7] to the intermediate $(2p2p,3pnd)$ states (ΔE_{CK}) was taken into account by performing a MCDF calculation with the optimal level scheme.[6] Consistent with our previous observations in Ne-like bismuth[2] the largest variations occur

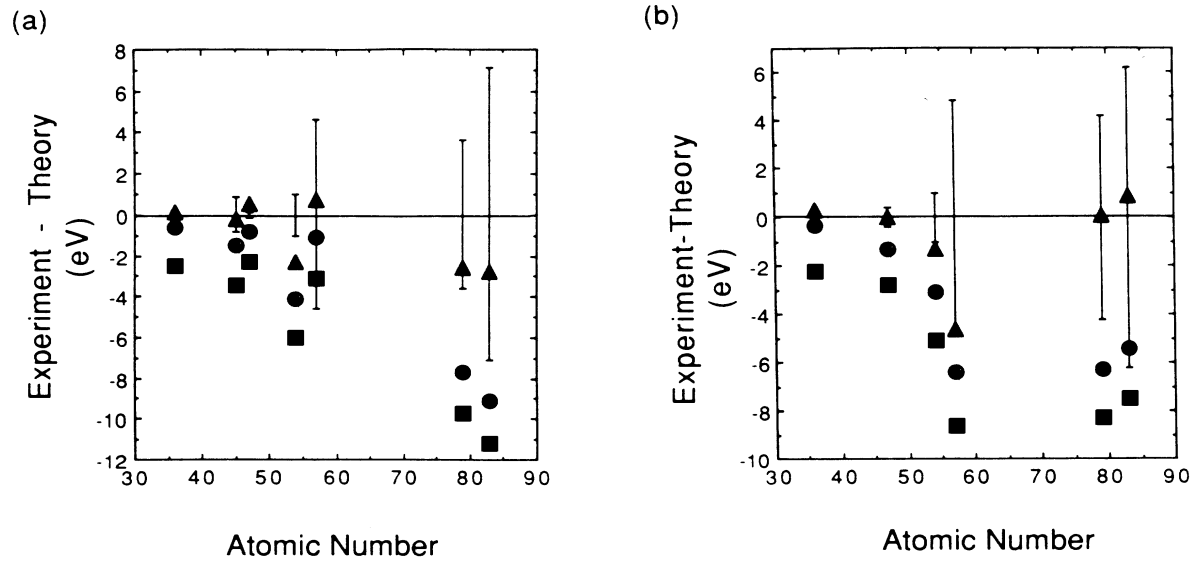

FIG. 4. (a) Variation between experiment and theory for the difference in the $(2s_{1/2},3p_{1/2})_1$-$(2p_{3/2},3s_{1/2})_1$ level separation for three different calculations. The squares indicate results from a MCDF calculation with screened self-energy terms but without an energy shift from Coster-Kronig fluctuation (ΔE_{CK}) of the $2s$ hole state. The solid circles represent the values from similar calculations including ΔE_{CK}. The triangles describe the MCDF results including ΔE_{CK} but using unscreened hydrogenic values for the self-energy terms. (b) Same kind of variation for the $(2s_{1/2},3p_{3/2})_1$-$(2p_{3/2},3s_{1/2})_1$ level separation.

on the Ne-like, $n=3$-2 transitions with an initial state having a $2s$ hole. Satellite contamination of these spectral lines was considered by fitting long-wavelength Gaussian profiles to the spectral features, and a shift to lower energy of these lines of ~ 1.3 eV was estimated due to these contributions. The variations in these transitions are interesting as they have the largest observed QED contributions, and the consistent variations between the data and the theory seem to imply that the empirical electron screening corrections used to calculate the effective many-electron Lamb-shift corrections from the hydrogenic calculations of Mohr[8] overestimate the electron shielding corrections. These variations are also indicated in the energy-level differences between the $2s$ hole states and the other Ne-like levels, and, as the systematic errors associated with the absolute energies are dominated by the uncertainties in the values for the foil location and the beam energy, as is indicated in Table II, a slightly more restrictive error estimate can be obtained on the energy-level differences. Thus in Figs. 4(a) and 4(b) we have plotted the differences of the experimental and theoretical values for the energy-level differences between the Ne-like $(2s_{1/2},3p_{1/2})_1$ and $(2s_{1/2},3p_{3/2})_1$ levels and the $(2p_{3/2},3s_{1/2})_1$ level for Kr(+26),[9] Rh(+35),

TABLE III. F-like gold $n=3$-2 transition energies. The F-like excited levels are denoted by their strongest configuration component which is labeled by its two holes in the L shell, which couple to form a state of intermediate angular momentum, and the excited electron with $n=3$ or 4 which couples to the core to form the total angular momentum. The individual electron spin-orbital states are indicated as follows: $nS\equiv ns_{1/2}$; $nP\equiv np_{3/2}$; $nP-\equiv np_{1/2}$; $nD\equiv nd_{5/2}$; $nD-\equiv nd_{3/2}$; $nF\equiv nf_{7/2}$; $nF-\equiv nf_{5/2}$. Numbers in parentheses are experimental errors.

Transition Upper state	Lower state	Measured (eV)	Rel. int.	Calculated (eV)	Difference (eV)	gf
$(2S\,2P;2\,3D)_{1/2}$	$2S$	10 628.1(5.5)	0.31	10 624.3	3.83	1.490
$(2P\,2P;2\,3D)_{5/2}$	$2P$	10 662.2(5.6)	0.31	10 670.0	−7.80	2.600
$(2P\,2P;2\,3D)_{1/2}$	$2P$			10 670.9	−8.72	2.100
$(2P-2P;1\,3D)_{3/2}$	$2P-$			10 651.6	10.53	0.096
$(2P\,2P;2\,3D)_{1/2}$	$2P$			10 643.4	18.76	0.400
$(2P-2P;2\,3D)_{3/2}$	$2P-$	10 699.4(5.6)	0.24	10 698.5	0.92	3.000
$(2P-2P;2\,3D)_{1/2}$	$2P-$			10 705.0	−5.54	1.600
$(2P\,2P;0\,3D)_{5/2}$	$2P$			10 710.5	−11.09	1.700
$(2P-2P;1\,3S)_{3/2}$	$2P$	11 562.2(6.4)	0.05	11 555.0	7.22	0.020
$(2P-2P;1\,3S)_{5/2}$	$2P$			11 575.5	−13.28	0.050
$(2S\,2P;2\,3P-)_{3/2}$	$2P$	12 167.6(7.1)	0.32	12 169.7	−2.15	0.160
$(2S\,2P;2\,3P-)_{1/2}$	$2P$			12 170.9	−3.34	0.640
$(2P-2P;1\,3D-)_{5/2}$	$2P$	12 398.5(7.3)	0.16	12 408.4	−9.93	0.440
$(2S\,2P-;1\,3D)_{3/2}$	$2P$			12 410.9	−12.41	1.250
$(2S\,2P-;1\,3D)_{1/2}$	$2P$			12 417.1	−18.63	0.590
$(2P-2P;2\,3D-)_{1/2}$	$2P$	12 434.6(7.4)	0.19	12 435.8	−1.25	0.620
$(2P-2P;2\,3D-)_{5/2}$	$2P$			12 438.3	−3.74	1.580
$(2P-2P;2\,3D-)_{3/2}$	$2P$			12 444.6	−9.98	1.300
$(2P-2P-;0\,3D-)_{3/2}$	$2P-$	12 478.0(7.4)	0.06	12 475.9	2.13	1.020
$(2S\,2P;2\,3P)_{3/2}$	$2P$	12 706.3(7.7)	0.15	12 704.7	1.56	0.230
$(2S\,2P;2\,3P)_{5/2}$	$2P$			12 712.5	−6.25	0.230
$(2S\,2P-;0\,3P)_{3/2}$	$2P-$			12 726.9	−20.61	0.100
$(2S\,2P-;1\,3P)_{3/2}$	$2P-$	12 784.5(7.8)	0.06	12 770.1	14.35	0.230
$(2S\,2P-;1\,3P)_{1/2}$	$2P-$			12 779.3	5.14	0.170
$(2S\,2S;0\,3P)_{3/2}$	$2S$			12 780.7	3.82	0.240
$(2S\,2P;1\,3P)_{5/2}$	$2P$			12 795.2	−10.69	0.270
$(2S\,2P;1\,3P)_{3/2}$	$2P$			12 803.1	−18.61	0.110
$(2S\,2P;2\,3D-)_{7/2}$	$2P$	12 865.4(7.8)	0.03	12 861.5	3.87	0.010
$(2P\,2P;2\,4D)_{3/2}$	$2P$	14 044.4(9.2)	0.06	14 041.4	3.02	0.140
$(2P\,2P;2\,4P)_{5/2}$	$2P$			14 046.1	−1.75	0.600
$(2P\,2P;2\,4F)_{5/2}$	$2P$	14 096.3(9.3)	0.01	14 092.4	3.85	0.007
$(2S\,2P;1\,4F-)_{3/2}$	$2S$			14 094.0	2.24	0.000
$(2S\,2P;1\,4F-)_{5/2}$	$2S$			14 095.6	0.64	0.001
$(2P\,2P;0\,4D)_{5/2}$	$2P$			14 103.7	−7.38	0.240

TABLE IV. Ne-like $n=3-2$ satellite transitions observed. Numbers in parentheses are experimental errors.

Transition sequence	Ion stage	Energy measured (eV)	Rel. int.	Energy calc.[a] (eV)	Energy calc.[b] (eV)
$2p_{3/2}$-$3s_{1/2}$	Na	9446.3(4.5)	0.39	9448.7	9450.1
$2p_{3/2}$-$3d_{3/2}$	Na	10317.7(5.2)	0.05		10315.8
$2p_{3/2}$-$3d_{5/2}$	Na	10480.8(5.4)	1.53	10484.1	10489.4
	Mg	10443.3(5.3)	0.43	10440.0	10437.3
$2p_{1/2}$-$3s_{1/2}$	Na	11310.2(6.2)	0.03	11331.1	11312.5
$2p_{1/2}$-$3d_{3/2}$	Na	12221.3(7.1)	0.58	12224.9	12227.3
	Mg	12189.4(7.1)	0.13	12181.7	12182.9
$2s_{1/2}$-$3p_{1/2}$	Na	12028.8(6.9)	0.23	12047.9	12030.4
$2s_{1/2}$-$3p_{3/2}$	Na	12538.7(7.5)	0.18	12563.1	12542.8
$2p_{3/2}$-$4d_{5/2}$	Na	13702.4	0.17		
	Mg	13604.6	0.06		

[a]UTA calculation (Ref. 11).
[b]MCDF-EAL calculation.

Xe(+45), La(+47), Au(+69), and Bi(+73).[3] As seen in these figures, in addition to the QED screening effects, configuration-interaction effect of the $2s$ hole states with doubly excited $(2p2p,3pnd)_1$ states are also important. However, by also turning off the screening of the hydrogenic self-energy, systematically better agreement between the theory and experiment is achieved. This is also indicated in lower Z Ne-like Ag(+37), Xe(+44), and La(+47) observed in tokamak plasmas.[10]

Although smaller in intensity, there are 13 features which have been identified as F-like. These are shown in Table III. All but three of the features are blended with other F-like lines and are therefore difficult to compare with the MCDF-EAL calculations. The general agreement is, however, good and all three of these features agree within the experimental error. Three features are composed of two close-lying F-like components and two of them are also in good agreement with theory. The line at 11562 eV is not in as good agreement but it is a very weak, broad feature.

Resolved Ne-like satellite features from the Na-like and Mg-like charge states are also observed and indicated in Table IV. There are a large number of unresolved spectral components in these features. Calculations have been made by Bauche-Arnoult *et al.*[11] based on the method of unresolved transition arrays (UTA's) in the spin-orbit split subarray limit for the $n=3$-2 satellite features. In addition, we have also carried out MCDF-EAL calculations and the energy of the strongest component, based on the gf values, into a line feature has been listed. Good agreement between the experimental and the theoretical values is observed except for the $2s$ hole-state transitions calculated in the UTA model where differences of about 20 eV are observed.

The only other prominent features observed in the spectra in Figs. 3(a) and 3(b) are two weak broad lines, at 1.1449 and 1.1496 Å, which can be assigned to a large set of unresolved O-like, $n=3$-2 transitions.

The authors are grateful to Roger Morales, Jay Gier, and Dave Leneman for their support in constructing and setting up the apparatus, and to the staff at GSI for their help in performing this experiment. This work was performed in part under the auspices of Gesellschaft für Schwerionenforschung and the U.S. Department of Energy by Lawrence Livermore National Laboratory under Contract No. W-7405-Eng-48.

[1]W. H. Goldstein, R. S. Walling, J. Bailey, M. H. Chen, R. Fortner, M. Klapish, T. Phillips, and R. E. Stewart, Phys. Rev. Lett. **58**, 2300 (1987).
[2]D. D. Dietrich, G. A. Chandler, P. O. Egan, K. P. Ziock, P. H. Mokler, S. Reusch, and D. H. H. Hoffman, Nucl. Instrum. Methods B **24/25**, 301 (1987).
[3]G. A. Chandler, Ph.D. thesis, University of California, Davis, 1988.
[4]D. D. Dietrich, G. A. Chandler, R. J. Fortner, C. J. Hailey, and R. E. Stewart, Phys. Rev. Lett. **54**, 1008 (1985).
[5]V. S. Nikolaev and I. S. Dmitreiv, Phys. Lett. **28A**, 227 (1968).
[6]I. P. Grant, B. J. McKenzie, P. H. Norrington, D. F. Mayers, and N. C. Pyper, Comput. Phys. Commun. **21**, 207 (1980); B. J. McKenzie, I. P. Grant, and P. H. Norrington, *ibid.* **21**, 233 (1980).
[7]M. H. Chen, B. Crasemann, N. Martensson, and B. Johansson, Phys. Rev. A **31**, 556 (1985).
[8]P. J. Mohr, Ann. Phys. (N.Y.) **88**, 52 (1974); Phys. Rev. Lett. **34**, 1050 (1975).
[9]J. E. Rice, E. S. Marmar, J. L. Terry, K. F. Daley, B. L. Whitten, R. S. Walling, J. H. Scofield, and M. H. Chen (unpublished).
[10]P. Beiersdorfer *et al.*, Phys. Rev. A **37**, 4153 (1988).
[11]C. Bauche-Arnoult, J. F. Wyart, and E. Luc-Koenig, Nucl. Instrum. Methods B **31**, 153 (1988).

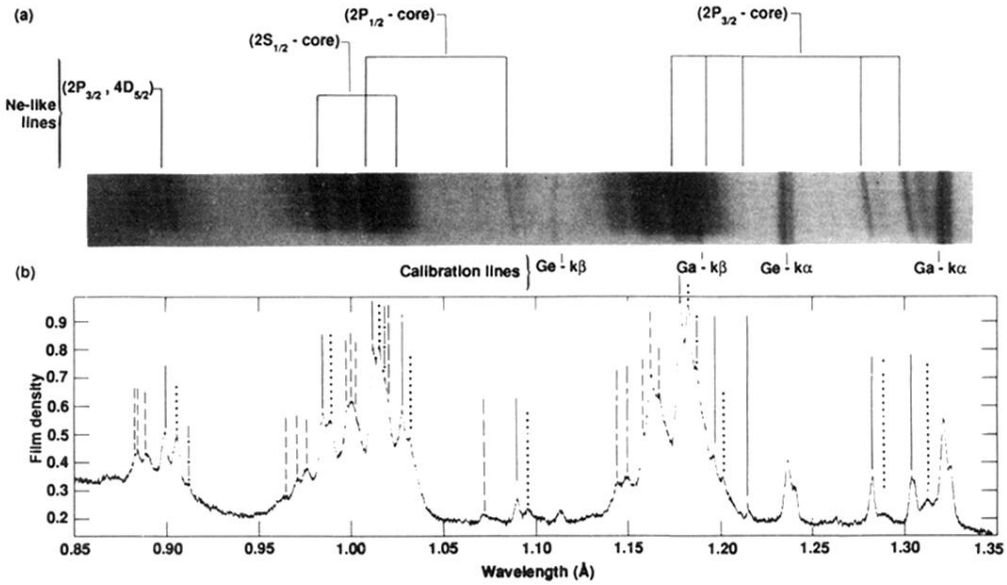

FIG. 3. (a) Raw film data of a gold x-ray spectrum taken with an indium antimony 220 crystal. (b) A densitometer trace of the spectrum formed by averaging densitometer scans along the gold x-ray lines. The lines are identified from a given charge state in the spectra as follows: ——, Ne-like; · · · ·, Na-like, —·—·—·, Mg-like; — — —, F-like; -----and O-like.